

# PERFORMANCE CHARACTERISTICS OF A REDUCED SOLIDITY LOW PRESSURE TURBINE

W. J. Solomon  
GE Aircraft Engines

**Keywords:** Turbine, Aerodynamics, Performance, Turbulence, Reynolds Number, Clocking

## Abstract

*The performance of a two stage reduced solidity low-pressure turbine was measured in a low-speed test facility and compared with results from a baseline turbine with conventional solidity levels. Both turbines were tested with clean inlet flow, and with a turbulence grid at inlet, to give a total of four configurations. Effects of Reynolds number and airfoil clocking were also investigated.*

*The low solidity turbine was found to have lower efficiency than the baseline when the inlet turbulence level was low. With increased inlet turbulence the low solidity turbine performed slightly better than the baseline. The low solidity turbine also performed slightly better than the baseline at low Reynolds number.*

*A significant variation in performance of the low solidity turbine was measured when the second stage nozzle was clocked circumferentially relative to the first. Increased inlet turbulence was found to reduce the clocking effect. Possible explanations for the observed clocking effects are discussed relative to surface hot-film boundary layer measurements and limited total pressure traverse data.*

## 1 Introduction

This paper describes work on low pressure (LP) turbine aerodynamics performed in the Aerodynamics Research Laboratory at GE Aircraft Engines. The low-speed research turbine (LSRT) was used as the test vehicle to investigate the con-

sequences of designing an LP turbine with lower solidity and hence higher loading than conventional design practice.

Around the time this work started there was evidence in the open literature that conventional turbine designs had higher than optimum solidity if the weight vs efficiency trade-off was considered (Cobley et al. [1] and Curtis et al. [2]). At the same time there were some warnings that high-lift designs may pose an unacceptable risk of complete separation and high loss, especially at low Reynolds number (Sharma [7]). The on-going attractiveness of solidity reduction to turbine designers is confirmed by the extreme measures being considered by some workers to control boundary layers on high lift airfoils. Ramesh et al. [5] demonstrate a possible benefit obtained by deliberately increasing surface roughness. Boundary layer suction and blowing concepts also continue to attract attention.

Accurate understanding of turbine efficiency is required for studies at the engine system level necessary to determine an optimum solidity. Halstead et al. [3], Schulte and Hodson [6] and others have demonstrated that the state of the boundary layer is a crucial factor in determining airfoil profile loss at the low Reynolds numbers at which LP turbines operate. On the airfoil shown in this paper, the blade surface boundary layer is laminar for at least 50 percent surface length. CFD that ignores boundary layer transition cannot be expected to correctly predict LP turbine performance trends.

Numerical prediction or experimental modeling of LP turbine flows must be made in a

representative turbulence environment because free-stream turbulence levels control the location of boundary layer transition. The author (reference [9]) demonstrated that transition onset can be predicted with reasonable accuracy if measured free-stream turbulence levels are available. A review of published data from cold-flow high speed rig tests by Hodson [4] found peak turbulence intensities in rotor wakes of 5-10% and between wakes of 3-5%. Sharma [7] reported turbulence measurements made in an engine that showed wake turbulence levels in the 16–23% range. The difference between these results partly reflects the difficulty of the measurement environment, but may be the result of real differences in the design of individual machines and the presence of combustor turbulence in Sharma's test. Non-linearity in the influence of turbulence on boundary layer transition reduces the importance of knowing the exact turbulence level at the high end of the scale (see [9]).

## 2 Test Vehicle

The LSRT is a two stage machine with an outlet guide vane row (Fig. 1). The rig has a vertical axis and air from the room enters through a calibrated bell-mouth at the top. A fine mesh screen and a layer of filter cloth ensure a clean, evenly distributed flow. Underneath the test floor (not shown in Fig. 1) a large centrifugal compressor draws air through the turbine. The compressor and turbine are both coupled through a gearbox to the same DC electric drive so that power generated by the turbine is recycled to help drive the compressor.

The design speed of the turbine is around 610 RPM; slight adjustments are made during a test to maintain constant Reynolds number. Low speed significantly reduces the cost of manufacturing and operating the test rig compared with conventional high speed testing. The Reynolds number is similar to that of an LP turbine at turbofan engine conditions. The Mach number is in the low subsonic range - not representative of engine conditions. This shortcoming is not crucial, unless strong shock-boundary layer interactions are ex-

pected in the product being simulated, provided allowance is made for the lack of compressibility in the design phase.

Vector diagrams and airfoils for this test were designed to be representative of a typical LP turbine stage in a large commercial turbofan engine. The maximum flow-path diameter is 1.524 m (60 inches). The slope of the outer casing was selected to fall in the range encountered in GE products. A sloped outer casing was manufactured so that secondary flow effects such as those calculated by Turner [10] could be studied. Since the flow in the LSRT is essentially incompressible, the flowpath area cannot vary in exactly the same way as the engine being simulated. The inner flowpath slope was adjusted to compensate.



**Fig. 1** The Low Speed Research Turbine (LSRT) in sloped end-wall configuration (Low Speed Research Compressor in background)

## 2.1 Blading design

Two sets of blading were designed for this test. Both sets of airfoils were designed for the same flow-path and the same vector diagrams and had similar axial chord. Solidity based on axial chord for the second stage nozzle was varied from 0.97 for the baseline machine to 0.74 for the low solidity blading by removing and re-designing airfoils. The other 3 rows were varied similarly to give an airfoil count reduction of around 22%.

More specific information regarding the second stage nozzle airfoil, including design suction surface velocity profiles, is given in Solomon [9].

## 2.2 Instrumentation

The temperature rise across this turbine is small because the speed is low. Consequently the drop in total temperature across the turbine could not be measured accurately enough to estimate the work done by the flow and a strain-gauge type torque meter was used instead. Inlet temperature, required for air property calculations, was measured with an array of RTDs mounted on the inlet screen ahead of the bell-mouth. A sixty-tooth gear and proximity sensor in the torque meter was used to provide a speed signal that was averaged using a precision HP counter to give rotational speed (RPM). Surface hot-film data acquisition was triggered by a once-per-rev signal obtained from an optical sensor aimed at reflective tape on the shroud of one of the rotating blade rows.

Pressure measurements were made with precision differential pressure transducers with a common reference pressure. An electronic barometer was used to obtain absolute pressure levels. Differential transducers gave better accuracy than subtracting measurements from multiple absolute transducers for the small differences being measured.

A cross-section of the LSRT with instrumentation planes denoted is shown in Fig. 2. Traversing behind stationary blade-rows is facilitated by a design that allows the blade-rows to be circumferentially clocked relative to the probe while the

rig is running. Radial traversing is performed using Rotadata® linear actuators.

Inlet total pressure was measured with pitot probes at station 0.9 at three different circumferential locations. As part of initial rig calibration, plane 0.9 was traversed in the span-wise direction over a range of rig conditions to measure the inlet boundary layers and any other flow non-uniformity. For clean-inlet testing the inlet total pressure probes were fixed mid-span and a correction coefficient based on the calibration measurements was applied to obtain the true inlet total pressure. Installation of a turbulence grid upstream of plane 0.9 complicated the measurement of inlet total pressure. Despite care taken to insert the grid in a repeatable fashion, small variations in the grid installation were found to cause unacceptably large variations in the measured inlet total pressure. The total pressure downstream of the grid was mapped out with probes at plane 0.9 over the full range of grid circumferential locations and a new calibration coefficient was calculated. A pressure upstream of the grid (at the mass-flow measurement plane) was used as the reference so that misalignment of the grid could not cause spurious measurements.

Exit total pressure was measured by radially traversing Kiel-head probes at 3 different circumferential locations in the Rotor 2 - OGV gap (plane 2.95). Calibration tests were performed to check for circumferential variation of exit total pressure at plane 2.95 - this was found to be small. To ensure maximum measurement repeatability, overall performance was calculated with the stationary bladerows and OGV fixed in a reference circumferential position.

Mass-flow was measured at a plane upstream of plane 0.9, not shown of Fig. 2. A sixty degree segment was mapped out with a pitot probe so that the the wake one of the six inlet struts could be measured accurately.

## 2.3 Measurement system accuracy

The measurement system accuracy can be estimated by approximating the expression for isentropic efficiency as follows

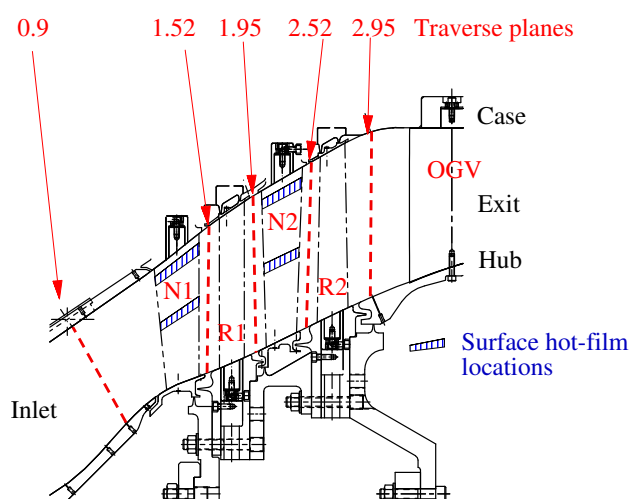


**Fig. 2** LSRT cross section. Instrumentation traverse planes in red

$$\eta = \frac{\tau \omega}{\dot{m} C_p T_0} \frac{P_0}{\Delta P} \frac{\gamma}{\gamma - 1} \quad (1)$$

This approximation is valid for  $\Delta P/P_0 \ll 1$ , a reasonable assumption in the LSRT. Since all terms in the simplified expression have exponents of unity, the overall uncertainty can be obtained by root-sum-square addition of the percentage uncertainties in the individual terms. Typical values for the individual terms are given in Table 1.

**Table 1** LSRT measurement system uncertainties (2 sigma/95% confidence) at design point

Variable	Symbol	% uncertainty
Mass flow	$\dot{m}$	$\pm 0.15$
Torque	$\tau$	$\pm 0.10$
Speed	$\omega$	$\pm 0.08$
Temperature	$T_0$	$\pm 0.07$
Inlet total pressure	$P_0$	$\pm 0.05$
Pressure drop	$\Delta P$	$\pm 0.01$
Total	$\eta$	$\pm 0.22$

The uncertainty quoted in Table 1 represents the total uncertainty; both bias errors and random variations are included. The uncertainty in measured efficiency  $\eta$  quoted in Table 2 below consists of random variation effects only, and includes a benefit due to repeated measurements. Build-to-build variations in bias errors are ex-

pected to be small and have not been accounted for.

## 2.4 Turbulence characteristics

Free-stream turbulence is an important variable for turbines with significant areas of laminar boundary layer flow. A square mesh grid was mounted in the duct upstream of the turbine inlet plane to augment the turbulence level.

Design constraints for the grid were; solidity less than 40%, minimum of 10 grid bars across the annulus and fully developed flow (or close to it) at the turbine inlet plane. These constraints lead to a grid of 4.17 mm square bar with a pitch of 17.73 mm. The flow distance from the grid to the leading edge of the first row of blading is approximately 20 times the grid pitch. Figure 3 shows a view of the turbulence grid installed in the LSRT. Predicted turbulence level was around 5 percent with an integral length scale of 7 mm.

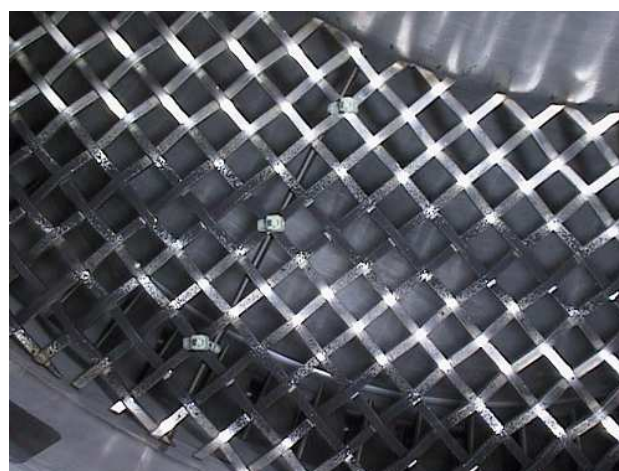


**Fig. 3** Turbulence grid installed in LSRT inlet duct

Measurements of the inlet turbulence at plane 0.9 were made with a two component "X" hot-wire and are plotted in Fig. 4. Turbulence was defined relative to the mid-span velocity to prevent the low velocities in the endwall boundary layers from magnifying the turbulence levels there. The casing endwall boundary layer is thicker than the hub boundary layer and has a more developed turbulence profile. Mid-span turbulence levels

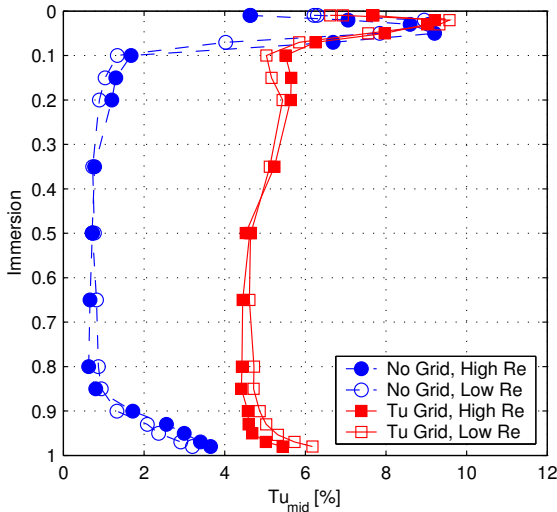


**Fig. 4** Turbulence level measured at inlet plane 0.9

generated by the grid were close to design intent and no undesirable flow instabilities were observed.

### 3 Performance Measurements

#### 3.1 Design Point

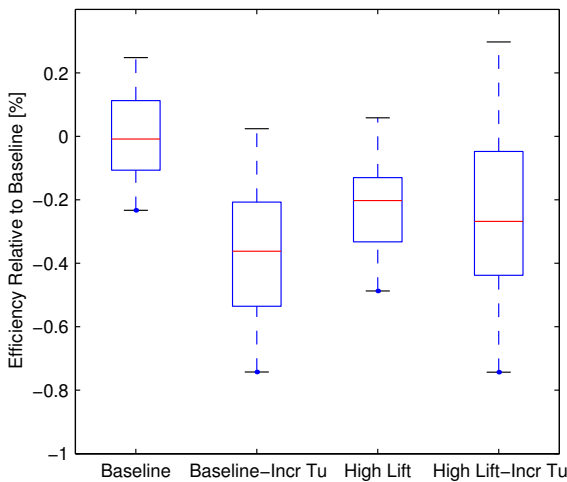


**Fig. 5** Overall efficiency at design point: Baseline and high-lift turbines, with and without inlet turbulence grid. Pressure drop across turbine for efficiency calculation does not include grid loss.

Data was taken in several phases for each

build. Overall performance data at the design point was taken early in each test and then throughout the testing to verify continued data integrity. At least 60 data-points were taken at design conditions for each configuration; more than sufficient to allow the statistical significance of measured differences between builds to be assessed. Multiple readings at any given operating point were used to reduce the effect of random variation and improve the precision of the overall performance measurements. Bias errors cannot be reduced by multiple readings. Differences between the test configurations that could introduce errors that would bias efficiency delta calculations include; the effect of rig disassembly and reassembly, variations in clearances and differences in inlet total pressure calibration due to the turbulence screen. The second and third possibilities were reduced as much as possible by careful measurement and calibration. A rebuild of one of the configurations was performed to verify the repeatability of the assembly process.

Figure 5 shows overall isentropic efficiency measurements at the design point for the four different configurations tested. Efficiency is plotted relative to the clean-inlet baseline solidity turbine. The mean level is indicated by the red-line in the blue box. The blue box represents 95% confidence limits and the black horizontal lines represent the extreme data points.

It is helpful to use a T-test to quantify the statistical significance of the measured differences between configurations. Table 2 shows results for selected combinations.

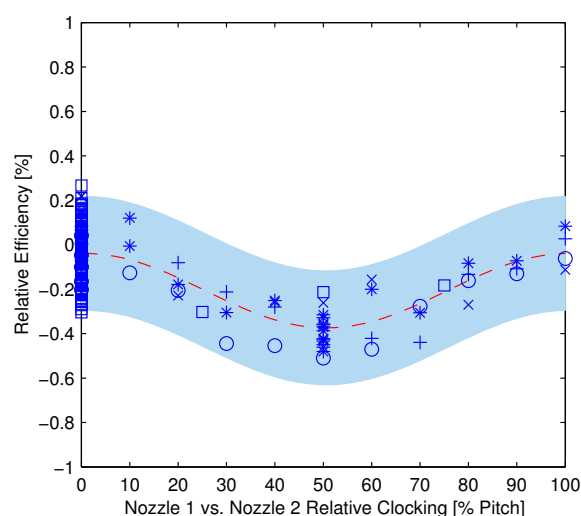
The high lift turbine performed slightly better than the baseline turbine with increased inlet turbulence levels. With clean inlet, the baseline turbine performed better. The baseline turbine suffers a significant degradation of performance with high inlet turbulence whereas the effect of increased turbulence on the low solidity turbine was too small to measure with confidence.

#### 3.2 Bladerow Clocking with High Lift

The LSRT was designed to allow adjustment of the relative circumferential location of the two

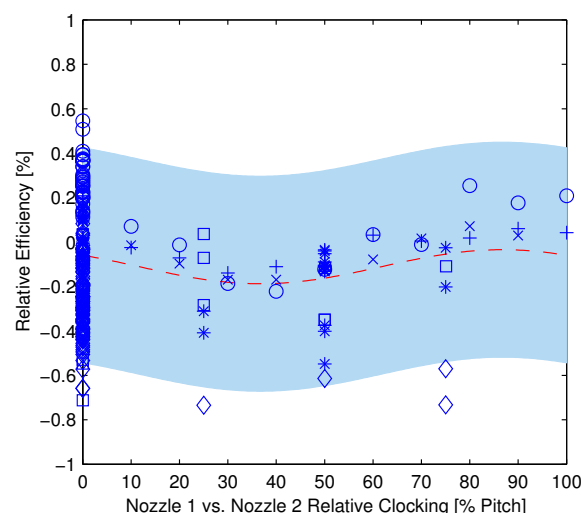
**Table 2** Measured efficiency deltas, including uncertainty

Configuration	$\Delta\eta$ [%]
Baseline	
Grid-No grid	$-0.37 \pm 0.06$
High Lift	
Grid-No grid	statistically indistinguishable
No Grid	
High lift - Baseline	$-0.22 \pm 0.04$
Tu Grid	
High lift - Baseline	$0.13 \pm 0.06$

**Fig. 6** Effect of stationary bladerow clocking on overall efficiency: Clean Inlet

stationary nozzle bladerows while running. The reduced solidity turbine was designed with equal numbers of nozzle airfoils so that the effect of clocking on overall performance could be studied.

Rotor airfoil counts were also equal in the two reduced solidity stages and in principle, a clocking effect could also have been measured by adjusting the rotor relative circumferential location. This was not attempted because rig disassembly would be required for each adjustment of the rotor airfoil angular location. Consideration of the rotor wake trajectory showed that the wakes from the first rotor are skewed as they pass through the second nozzle such that the downstream rotor is never predominately either in or

**Fig. 7** Effect of stationary bladerow clocking on overall efficiency: Turbulence Grid Inlet

out of the wake of the upstream rotor for any given clocking arrangement. Instead, the influence of the upstream rotor would simply move up and down the span of the downstream rotor, with little net effect on profile loss expected.

Figures 6 and 7 show the measured variation in turbine efficiency as a function of circumferential position of the second nozzle relative to the first. The red dashed line is the result of a sine function regression fit to the data. The light blue shaded region represents 95% confidence limits based on the nominal (0%) clocking data. Figure 6 shows that the overall turbine efficiency varies by almost 0.4% with clean inlet flow. This variation must be almost entirely the result of change in the second stage nozzle efficiency, although the possibility that clocking the potential field of the second nozzle had a detrimental effect on the upstream rows has not been ruled out. Coincidentally, the nominal clocking orientation (used for all other overall performance measurements) was found to be close to optimum.

With raised inlet turbulence, the clocking effect is reduced by more than 50% (Fig. 7). This result suggests that the efficiency variation with clocking observed in Fig. 6 was primarily due to the wake of the first nozzle interacting with the second, and is not a potential flow effect.

Comparison of figures 6 and 7 at 50% clocking shows that increased inlet turbulence enhances performance. The effect of turbulence at 0% clocking has already been shown to be too small to measure (Fig. 5). Assuming the efficiency change occurs in the second nozzle, the largest delta would be expected to correlate with the largest change in turbulence felt by that row. This suggests that the 50% clocking orientation places the second nozzle clear of the wake of the first so it feels a large change in turbulence when the grid is added.

### 3.3 Behaviour at Low Reynolds Number

Testing was performed at Reynolds numbers ranging between 120% and 35% of the design level. Figure 8 shows the overall efficiency variation with Reynolds number for the baseline and low solidity turbines under high inlet turbulence conditions. Over the range tested, the low solidity turbine showed efficiency degradation with reduced Reynolds number similar to the baseline turbine. Experimental uncertainty increases as Reynolds number decreases, and the scatter in the baseline turbine data at low Reynolds number reduces confidence slightly. An increased number of readings was taken during the low solidity testing to compensate.

Not shown in this paper, the sensitivity of efficiency to low Reynolds number was found to be higher with clean inlet. High inlet turbulence was found to reduce the loss in efficiency at low Reynolds numbers for both the baseline and high solidity turbine.

## 4 Flow Details

Detailed measurement of the flow were taken to help understand and explain the trends in overall efficiency shown above.

### 4.1 Surface Boundary Layers

Surface mounted hot-film gauges were used to measure the variations in time of shear stress. Results presented here are from the suction surface of the second stage nozzle. Twenty-five sensors

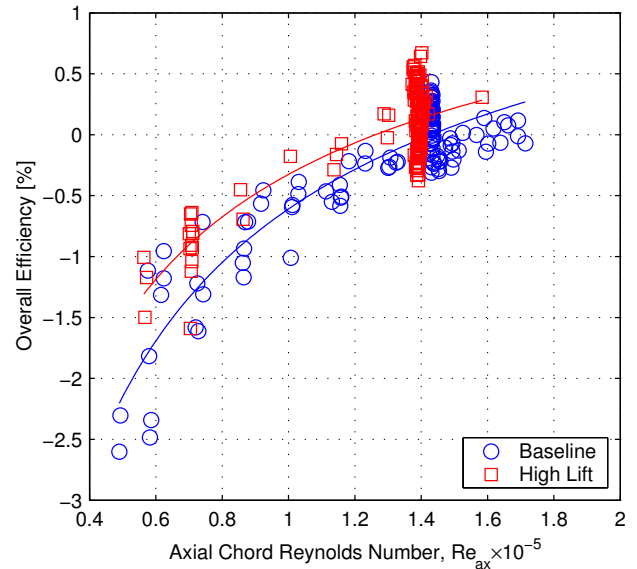


**Fig. 8** Variation of Efficiency with Reynolds Number: Turbulence Grid Inlet

were spaced along the mid-span streamline at a pitch of 2.54 mm.

The hot-film sensors were operated in constant temperature mode using standard TSI® model 100 anemometer bridges. Phase-lock average data was acquired at 50 kHz with low pass anti-aliasing filtering at 20 kHz. Square wave tests indicated the frequency response of the sensors was around 30 kHz, which is around 25 times blade pass frequency.

The hot-film sensors were not calibrated to yield a quantitative measure of shear stress (this is difficult when the flow is switching from laminar to turbulent). Instead, a signal proportional to the shear stress was produced following the method described in Solomon [9]. This signal was then further processed to calculate turbulent intermittency using the turbulent intermittency detection algorithm described in Solomon [8]. For unsteady measurements such as these, intermittency is defined as the probability of turbulent flow being measured at a given point in space-time. An intermittency level of 1.0 indicates fully turbulent boundary layer flow. Careful interrogation of the shear stress signals can reveal evidence of laminar separation although this is hindered by uncertainty in the zero skin friction measurement.

Figure 9 presents processed surface hot-film data time-space contour plots for three different configurations of the low solidity turbine. The space-time plots show dimensionless surface distance on the horizontal axis and time normalized by the blade passing period on the vertical axis. The slope of the trajectory of a flow feature on the time-space plot indicates the propagation velocity of the feature.

In general, an intermittency level of zero is observed over the front 50-70% of the blade surface (shown in blue), indicating fully laminar flow. The turbulence grid case in the lower part of the figure is the exception. That case has a region of slightly elevated intermittency between 20 and 30% surface distance. This is caused by spurious identification of fluctuations in the laminar boundary layer as turbulence and should be ignored. This buffeting of the laminar boundary layer does not cause boundary layer transition onset in this region of strong acceleration.

It is convenient to define transition onset as the 10% intermittency line (the first change from dark blue to the next shade). The transition onset line moves forward and aft on the blade surface with time, in phase with the passing wakes. The case with the turbulence grid (bottom of Fig. 9) has the earliest transition onset; fluctuating between 50 and 60% surface distance. Transition onset is furthest forward when influence of the first stage rotor is strongest and moves aft between rotor wakes. The case at the top of the figure (No Grid, Clocked 50%) has the lowest turbulence level at the inlet to the second nozzle, and has the latest transition onset; ranging from 58 to 70% surface distance.

The end of transition is conveniently defined as the 80% intermittency contour. End of transition occurs first in the wake-influenced region - interestingly at around the same point, 65% surface distance, regardless of the inlet turbulence level. Length of wake induced transition increases with turbulence level because the onset point moves forward.

Between wakes, the end of transition varies considerably depending on the free-stream turbulence level. For the two cases with increased free-

stream turbulence transition between wakes is not complete by the end of the sensor array. The “No Grid, Clocked 50%” case has a more rapid transition between wakes. Inspection of the individual traces and time-average shear stress levels indicated possible laminar separation between wakes for this case. Steady state calculations predicted laminar separation around 65% surface length. Reattachment of fully turbulent flow that has undergone transition in a separated shear layer is a likely explanation for the high levels of intermittency towards the trailing edge of the upper case compared with the lower two.

## 4.2 Endwall Secondary flows

Total pressure traverse measurements made with a Kiel head probe at the exit of the first nozzle (plane 1.52) are presented. Figures 10 and 11 show contours of total pressure loss normalized by turbine inlet dynamic head. A significant loss core is observed near the outer wall. This feature is presumably a secondary flow vortex which is augmented by the thick casing boundary layer (Fig. 4).

Figure 10 shows that solidity does not have a strong effect on the size of the vortex core, but does change the interaction between this vortex and the blade surface boundary layer. The high-lift airfoil shows significant thickening of the wake just below the vortex trajectory. Figure 11 shows that increased free-stream turbulence smears out the secondary flow vortex and mixes it with the locally thickened wake.

## 5 Discussion

The overall efficiency trends are generally similar to expectations. The baseline airfoils were close to laminar-flow design at low inlet turbulence levels; increased turbulence moved the predicted transition point far forward (Solomon [9]). This explains the strong effect of turbulence on the overall efficiency of the baseline turbulence. Steady flow calculations show that transition does not move far with changing turbulence on the low solidity airfoil - at high turbulence

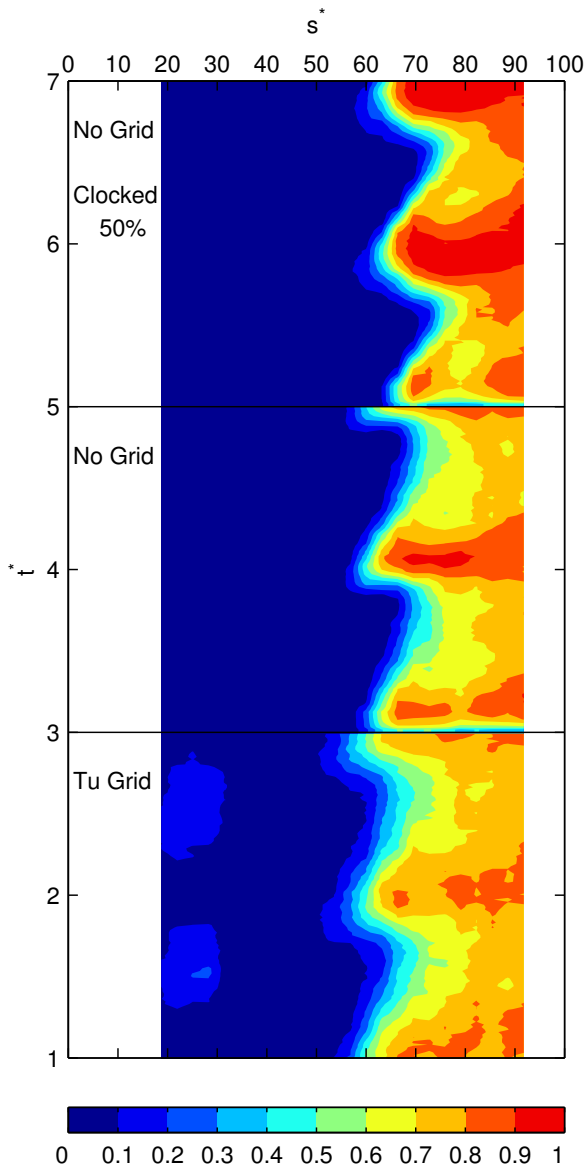


**Fig. 9** Surface hot film measurements on low solidity second stage nozzle

transition is prevented from moving forward by strong acceleration on the front part of the airfoil, at low turbulence a small laminar separation bubble between 65 and 70% surface distance limits the downstream movement of transition. Recall that the effect of inlet turbulence on the low solidity turbine was too small to measure.

The effect of clocking on the low-solidity design is not so easily explained. Two steady flow calculations with transition onset on the second stage nozzle at 50% and at 70% surface distance can only explain a change in overall efficiency of

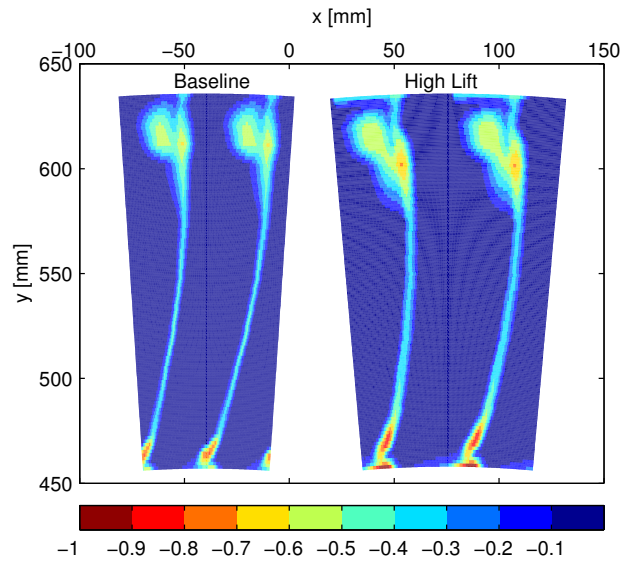


**Fig. 10** Effect of solidity on total pressure loss coefficient at plane 1.52 (N1 exit): Clean inlet

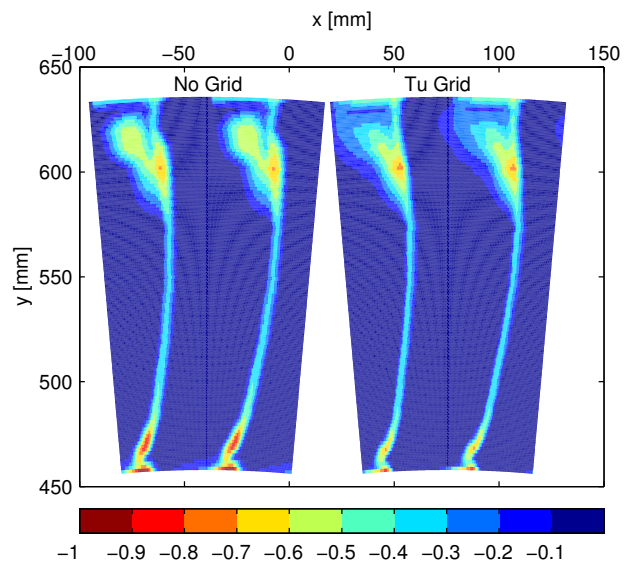


**Fig. 11** Effect of inlet turbulence on total pressure loss coefficient at plane 1.52 (N1 exit) : High lift configuration

around 0.23%. Since the time average change in transition onset location measured with the surface hot-films is less than the 20%, there is little hope of explaining the 0.4% change in overall efficiency measured with clean inlet. To add further difficulty, it is easily confirmed that transition onset moves in the opposite direction to that

required to explain the efficiency trend.

The clocking effect is significantly reduced under increased turbulence conditions (Fig. 7). This suggests the circumferential location of the potential flow-field of nozzle 2 does not alter the performance of the upstream blade-rows. The measurements show that it is beneficial to bathe the downstream nozzle in the wake of the upstream nozzle, despite the loss in efficiency that must be incurred as transition moves forward with the increased turbulence. The second stage nozzle loss may be reduced as a result of operating in the low inlet dynamic head region of the first nozzle wake. Turbulence would disperse the wake and reduce this proposed mechanism. The final two figures hint that secondary flow may also play a role.

## 6 Conclusions

- Feasibility of a low solidity turbine design was demonstrated
- The low solidity design out-performed the baseline in high inlet turbulence conditions
- A small efficiency penalty was observed at design point with clean inlet flow; this must be balanced against the weight reduction benefit
- Efficiency of the low solidity design was competitive with the baseline at low Reynolds number
- Efficiency is best when the second nozzle is clocked so it is bathed by the wake of the first
- The clocking effect was weakened by high inlet turbulence
- An interaction between the secondary flow vortex and the blade surface boundary layer was observed and indicates an area for future investigation

## 7 Acknowledgements

The Author's contribution to this work was supported by the NASA Lewis Low Pressure Turbine Research Program (grant number NCC3-588, 1998) administered by Dr. David Ashpis and by GE Aircraft Engines. The GEAE team included David Halstead, Rob Beacock, Bill Groll,

Don Menner, David Cherry and David Wisler. The Author was an employee of the Ohio Aerospace Institute for the duration of this program.

TSI® is a registered trademark of TSI Incorporated. Rotadata® is a registered trademark of Rotadata Inc.

## References

- [1] Cobley K, Coleman N, Siden G, and Arndt N. Design of a new three stage low pressure turbine for the BMW Rolls Royce BR715 turbofan engine. ASME Paper 97-GT-419, Orlando, Florida, 1997.
- [2] Curtis E. M, Hodson H. P, Baniaghbal M. R, Denton J. D, and Howell R. J. Development of blade profiles for low pressure turbine applications. ASME Paper 96-GT-358, International Gas Turbine and Aero-engine Congress and Exposition, Birmingham, UK, 1996.
- [3] Halstead D. E, Wisler D. C, Okiishi T. H, Walker G. J, Hodson H. P, and Shin H. Boundary layer development in axial compressors and turbines: Parts 1–4. *ASME Journal of Turbomachinery*, Vol. 119, No 1-3, pp 114–139, 225–237, 426–444, Jan–July 1997.
- [4] Hodson H. P. Bladerow interactions in low pressure turbines. *Proc Blade Row Interference Effects in Axial Turbomachinery Stages*, pp 1–62. von Karman Institute for Fluid Dynamics, February 1998. Lecture Series 1998-02.
- [5] Ramesh O. N, Hodson H. P, and Harvey N. W. Separation control in ultra-high lift aerofoils by unsteadiness and surface roughness. September 2001. Proc. 15th International Symposium on Air Breathing Engines, Bangalore, Paper No. 2001-1096.
- [6] Schulte V and Hodson H. P. Prediction of the becalmed region for LP turbine profile design. *ASME Journal of Turbomachinery*, Vol. 120, No 1, pp 28–35, January 1998.
- [7] Sharma O. Impact of Reynolds number on LP turbine performance. *Proc Minnowbrook Workshop on Boundary Layer Transition in Turbomachines*, pp 65–69. Syracuse University, New York, June 1998. NASA / CP–1998-206958.
- [8] Solomon W. J. *Unsteady Boundary Layer Transition on Axial Compressor Blades*. PhD thesis, University of Tasmania, Tasmania, Australia, August 1996.
- [9] Solomon W. J. Effects of turbulence and solidity on the boundary layer development in a low pressure turbine. ASME Paper 2000-GT-0273, Munich, June 2000.
- [10] Turner M. G. Multistage turbine simulations with vortex-blade interaction. ASME Paper 95-GT-288, Houston, Texas, 1995.